Superwettable PVDF/PVDF-g-PEGMA Ultrafiltration Membranes

ACS OMEGA

http://pubs.acs.org/journal/acsodf

Article

# Superwettable PVDF/PVDF-*g*-PEGMA Ultrafiltration Membranes

Qidong Wu, Alberto Tiraferri, Tong Li, Wancen Xie, Haiqing Chang, Yuhua Bai, and Baicang Liu*

Cite This: *ACS Omega* 2020, 5, 23450−23459

Read Online

ACCESS | Metrics & More | Article Recommendations

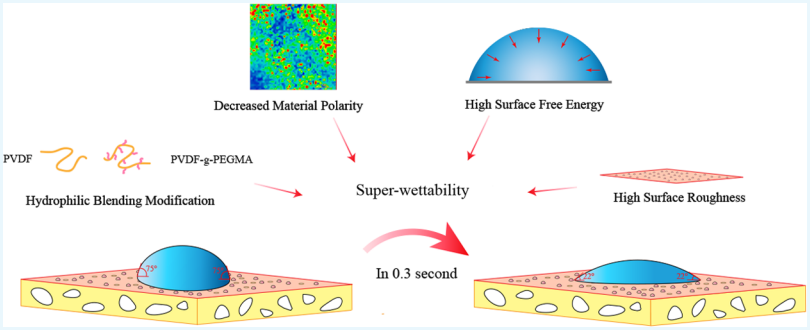


**ABSTRACT:** Poly(vinylidene fluoride) (PVDF) is a common and inexpensive polymeric material used for membrane fabrication, but the inherent hydrophobicity of this polymer induces severe membranes fouling, which limits its applications and further developments. Herein, we prepared superwettable PVDF membranes by selecting suitable polymer concentration and blending with PVDF-*graft*-poly(ethylene glycol) methyl ether methacrylate (PVDF-*g*-PEGMA). This fascinating interfacial phenomenon causes the contact angle of water droplets to drop from the initial value of over 70° to virtually 0° in 0.5 s for the best fabricated membrane. The wetting properties of the membranes were studied by calculating the surface free energy by surface thermodynamic analysis, by evaluating the peak height ratio from Raman spectra, and other surface characterization methods. The superwettability phenomenon is the result of the synergetic effects of high surface free energy, the Wenzel model of wetting, and the crystalline phase of PVDF. Besides superwettability, the PVDF/PVDF-*g*-PEGMA membranes show great improvements in flux performance, sodium alginate (SA) rejection, and flux recovery upon fouling.

## 1. INTRODUCTION

Since the large-scale commercial production of membranes was made possible through phase separation techniques, membrane-based separation technologies have developed rapidly and are currently used in many industrial sectors.[1,2] Poly(vinylidene fluoride) (PVDF) is a widely adopted membrane material. While PVDF has robust and flexible structures, its inherent hydrophobicity is the main obstacle for its wider applicability. For example, poor surface wetting may cause severe membrane fouling in the water- and wastewater-treatment fields. As a result, the membranes' service life would be reduced, and the cost of the whole process would increase. Therefore, much effort has been devoted to improving the hydrophilicity of PVDF membranes.[3−6]

Numerous studies have been published focusing on strategies to realize surface customization of PVDF membranes; among the effective methods currently applied are surface coating, surface grafting, and blending.[7−11] Blending is the most common method due to its simple operation, achieved material stability, and adequate modification results.[12] Among the materials used for blending with PVDF, amphiphilic copolymers have shown good compatibility with the PVDF matrix and are deemed as successful blending additives.[13,14] Several amphiphilic copolymers were synthesized using atom transfer radical polymerization (ATRP), and then blended with membrane materials.[12,15−17] Specifically, PVDF-*graft*-poly(ethylene glycol) methyl ether methacrylate (PVDF-*g*-PEGMA) is a derived amphiphilic copolymer synthesized using ATRP, which was blended with PVDF to enhance the hydrophilicity, flux, and antifouling performance of PVDF membranes.[18,19]

Theoretical models exist that allow the investigation and description of the hydrophilic membrane surfaces, such as those centered around surface tension.[20−22] Young proposed a wetting model based on ideal surfaces, while wetting models applicable on rough surfaces include the Wenzel model and the Cassie model.[23,24] Each model has its own applicabilities and limitations.[25] When studying the physicochemical properties of

**Received:** July 17, 2020
**Accepted:** August 25, 2020
**Published:** September 3, 2020

the membrane surface, the extended DLVO (XDLVO) theory can be applied to determine interfacial tensions and free energies.[20,21] These theories and models can provide a rationalization for the wetting behavior of the membrane surfaces, before and after modification or functionalization.

That being said, discussion of modified PVDF membranes' wettability properties has been very limited in previous studies. Moreover, the results of hydrophilic modifications for PVDF membranes were generally limited to a small reduction in the contact angle and an increase in water flux. Some recent studies focused on the hydrophilic modification of the PVDF membrane are listed in Table 1. In the previous study, we found that membranes with enhanced hydrophilicity were fabricated by changing the polymer concentration in the casting solution.[26] Following this line of thought, two superwettable modified PVDF membranes were successfully fabricated using lower polymer concentration in this study, the achieved outstanding improvement in wettability were studied and the relevant effects accounting for this phenomenon were investigated in details. In particular, chemical, physical, and structural features were studied and their combined influence on the surface wettability behavior was rationalized within the Wenzel model of wetting. The performances of the membranes were also evaluated under ultrafiltration conditions, allowing to draw a connection between the surface physicochemical characteristics to the membrane behavior when applied for the filtration of contaminated aqueous streams.

**Table 1. Wettability Performances of Several Hydrophilic Modified PVDF Membranes**

| membrane ID | modification method | additive | CA variation (deg) | time (s) |
|---|---|---|---|---|
| PVDF/PMAA[27] | in suit blending | PMMA | 84.8−75 | 300 |
| PVDF-*cl*-PVP[28] | cross-linking reaction | PVP | 70−0 | 45 |
| PVDF[29] | graft | GMA | 48 | static |
| PVDF-*g*-PEGMA 19 h[30] | blending | PVDF-*g*-PEGMA | 73−33 | 180 |
| PVDF-*g*-PEGMA[31] | blending | PVDF-*g*-PEGMA | 69−20 | 35 |
| PVDF-*g*-PEGDMA[32] | graft | PEGDMA | 59−0 | 15 |

## 2. MATERIALS AND METHODS

**2.1. Chemicals and Materials.** PVDF ($M_w$ = 534 K), 1-methyl-2-pyrrolidinone (NMP, 99.5%), 4-4′-dimethyl-2-2′-dipyridyl (DMDP, 99.5%), PEGMA (500 g/mol), copper(I) chloride (CuCl, ≥99.995%), silicone oil, *N*,*N*-dimethylacetamide (DMAc, 99%), sodium alginate (SA, Halal grade), and sodium chloride (NaCl, ≥99.0%) were purchased from Sigma-Aldrich (St. Louis, MO). Diiodomethane (99%) was purchased from Macklin (Shanghai, China). Glycerol (99.7%) was purchased from VWR (PA). Formamide (99%) and ethylene glycol (99%) were purchased from Kelong (Chengdu, China). Deionized water was supplied by an ultrapure water system from Ulupure (Chengdu, China) and was optimized with a previously reported process.[33]

**2.2. Synthesis of the Graft Copolymer PVDF-*g*-PEGMA.** As shown in previous studies, the synthesis steps of PVDF-*g*-PEGMA were as follows: first, NMP (40 mL) and PVDF (5 g) were placed in a conical flask, and then heated to 50 °C, stirring until the polymer was completely dissolved. The flask was cooled to room temperature. Then, PEGMA (50 mL), DMDP (0.23 g), and CuCl (0.04 g) were added to the flask. Immediately after the dosage, the reaction mixture was bubbled with nitrogen for 30 min and stirred at 200 rpm. The flask was sealed with a rubber septum, protecting the ATRP from oxygen in the air.[17] The conical flask was heated to 90 °C in a silicone oil bath and stirred for 19 h.[30] The resulting copolymer mixture was sealed and stored at room temperature.[26,34]

**2.3. Membrane Casting.** The organic solvents, copolymer, and the PVDF power were added to the flask based on the composition listed in Table 2. Then, the casting solution was stirred at 300 rpm at 60 °C until the chemicals were completely dissolved. The casting solution was degassed for at least 2 h until no bubbles were observed. Then, the solution was cast as a thin film on a first-grade surface optical glass using an 8-inch-wide doctor blade (Universal blade applicator, Paul N. Gardner Company, Inc., Pompano Beach, FL) with a blade gate height of 200 $\mu$m. The glass was then soaked in deionized water at room temperature for 48 h. Some of the fabricated membranes were stored in 4 °C DI water, while the rest was air-dried for 24 h. All of the membranes were cast in an air-conditioned room with set values of both temperature and humidity. The temperature was set to 25 °C while the humidity was set to be ∼45%.

**Table 2. Composition of the Casting Solutions[a]**

| membrane ID | PVDF (g) | DMAc (g) | NMP (g) | PVDF-*g*-PEGMA (g) | PVDF-*g*-PEGMA/PVDF wt/wt (%) |
|---|---|---|---|---|---|
| PVDF1 | 12 | | 88 | 0 | 0 |
| PVDF2 | 12 | 86.2 | | 1.8 | 15 |
| PVDF3 | 12 | | 86.2 | 1.8 | 15 |

[a]PVDF1 is a pure PVDF membrane.

**2.4. Model Foulant.** To evaluate the antifouling performance of the membrane, we used sodium alginate (SA) as a model extracellular polymeric substance (EPS).[35] The 2 g/L SA stock solution was prepared using deionized water and stored at 4 °C. In the fouling test, the SA stock solution was diluted to 20 mg/L. The concentration of SA in permeate was measured using the UV−vis spectrometer (Thermo Orion Aquamate 8000) with a fixed wavelength of 220 nm.

**2.5. Contact Angle Measurements and Surface Tension Calculations.** The contact angles of different liquids on the surface of the membranes were observed with a KRÜSS DSA 25S measuring apparatus (KRÜSS GmbH, Germany) using the sessile drop method.[36] The samples were vacuum-dried for 24 h before measurement. For each experiment, the dynamic contact angle of the probe liquid (2 $\mu$L) was recorded by a video camera attached to the goniometer, which was set to 50 images per second. The images were taken starting from the precise instant when droplets were placed on the sample surface. Ten spots in different positions on each sample were picked for this experiment, and the maximum and the minimum values were discarded when taking the average value.

The physicochemical properties of the fabricated flat sheet membranes, including the surface free energy, were calculated using the results based on the XDLVO theory.[20] According to this theory, the surface tension parameters, $\gamma_s^{LW}$, $\gamma_s^+$, $\gamma_s^-$, and $\gamma_s$ of the membrane surface can be calculated by measuring the contact angles using three probe liquids (l) with known surface


https://dx.doi.org/10.1021/acsomega.0c03429
ACS Omega 2020, 5, 23450−23459

tension parameters ($\gamma_l$) and solving a set of three Young–Dupré equations.

$$\gamma = \gamma^{LW} + \gamma^{AB} \quad (1)$$

$$\gamma^{AB} = 2\sqrt{\gamma^+\gamma^-} \quad (2)$$

$$(1 + \cos\theta)\gamma_l = 2\left(\sqrt{\gamma_s^{LW}\gamma_l^{LW}} + \sqrt{\gamma_s^+\gamma_l^-} + \sqrt{\gamma_s^-\gamma_l^+}\right) \quad (3)$$

The subscripts l and s refer to the liquid and the membrane, respectively. While $\gamma$ represents the total surface tension, $\gamma^{LW}$ is the Lifshitz–van der Waals components, $\gamma^{AB}$ is the Lewis acid–base components, and $\gamma^+$ and $\gamma^-$ are the electron acceptor and the electron donor components of the $\gamma^{AB}$ parameter, that is, the polar portion of the $\gamma$. In this study, apolar liquid diiodomethane, and polar liquids water, glycerol, formamide, and ethylene glycol, were selected as test liquids to calculate the surface free energy of the membranes. The calculation procedures have been described in detail in previous studies.[20,37] Two probe liquids, DI water (polar probe liquid) and diiodomethane (apolar probe liquid), were always the same for all of the samples. The third probe liquid was selected among glycerol, ethylene glycol, and formamide based on the suitability for each membrane surface. The surface tension parameters of the probe liquids are listed in Table 3.

**Table 3. Surface Tension Components (mJ/m$^2$) at 20 °C and $Q_r$ ($\gamma_l^-/\gamma_l^+$) of Probe Liquids Used in the Study**

| liquid | $\gamma_l$ | $\gamma_l^{LW}$ | $\gamma_l^{AB}$ | $\gamma_l^+$ | $\gamma_l^-$ | $Q_r$ |
|---|---|---|---|---|---|---|
| water | 72.8 | 21.8 | 51 | 25.5 | 25.5 | 1 |
| diiodomethane | 50.8 | 50.8 | 0 | ≈0 | 0 | |
| glycerol | 64 | 34 | 30 | 3.92 | 57.4 | 14.64 |
| formamide | 58 | 39 | 19 | 2.28 | 39.6 | 17.37 |
| ethylene glycol | 48 | 29 | 19 | 3 | 30.1 | 10.03 |

**2.6. Membrane Characterization.** X-ray photoelectron spectroscopy (XPS, Axis Ultra, Kratos Analytical Ltd., U.K.) was used to probe the elemental composition of the membrane surface. The range of the scanning electron binding energy was 0–1200 eV, and spectra with 1 eV scanning resolution were obtained. Images of membrane morphologies were acquired using field-emission scanning electron microscopy (FESEM, JSM-7500F, JEOL Ltd., Tokyo, Japan). Samples were fractured for cross-sectional imaging after being frozen in liquid nitrogen for 3 min. The membrane samples were sputter-coated with a ~2 nm gold layer (Q150R-ES, Quorum, U.K.) before imaging under an accelerating voltage of 5 kV. The spectra of Fourier-transform infrared attenuated total reflectance (ATR-FTIR, Alpha, Bruker) were collected over the range of 650–4000 cm$^{-1}$ with a resolution of 2 cm$^{-1}$ for 64 scans to characterize the chemical bonds on the surface of the fabricated membranes. The thickness of the membrane was measured with an electronic digital micrometer (Marathon watch company LTD, Canada). The surface roughness was determined using atomic force microscopy (AFM, Multimode 8, Bruker, Germany); sample areas of 5 $\mu$m × 5 $\mu$m were scanned for at least 2 times. Changes in the melting enthalpy of the membranes as a function of temperature were analyzed with a differential scanning calorimeter (DSC, TA Instruments Q2000). Samples were heated from 30 to 220 °C at a rate of 10 °C/min.[38] Raman spectra (DXR2xi Raman Imaging Microscope, Thermo Fisher) were acquired to identify the characteristic bands of different crystalline phases of PVDF in the fabricated membranes. The peak height ratio analysis of the membrane was performed using a 455 nm laser with a step length of 0.1 $\mu$m on the surface of 5 $\mu$m × 5 $\mu$m samples.

The permeability and antifouling performance of the membranes were measured through filtration experiments.[30,31] The experiments were carried out with a dead-end filtration system that included a filtration cell (200 mL; Amicon 8200, Millipore) and a dispensing vessel (5 L), at a constant pressure of 0.07 MPa at room temperature. The circular membrane samples had an effective area of 28.7 cm$^2$. The weight of the filtrate was recorded every minute. The flux was computed as L m$^{-2}$ h$^{-1}$. For each filtration experiment, the membrane was measured using DI water, 10 mmol/L NaCl condition solution, and SA model fouling solution in sequence. The recovery flux was measured after the membrane was physically cleaned for 1 min using a constant flow of DI water (2.7 L/min) after the fouling test. The flux for DI water, SA feed solution, and DI water in the recovery period was recorded as $J_{w1}$, $J_p$, and $J_{w2}$, respectively. The permeability of the membranes was measured for predetermined time or the time needed to filter 4 L of the feed solution, if lower than a set time. During the fouling test, the feed solution in the filtration cell was stirred at 200 rpm to minimize the concentration polarization. The flux recovery ratio (FRR), total flux decline ratio ($DR_t$), reversible flux decline ratio ($DR_r$), and irreversible flux decline ratio ($DR_{ir}$) were calculated with the following equations using an average value from separate tests for each membrane sample.[26,31]

$$FRR = \frac{J_{w2}}{J_{w1}} \times 100\% \quad (4)$$

$$DR_t = \left(1 - \frac{J_p}{J_{w1}}\right) \times 100\% \quad (5)$$

$$DR_r = \left(\frac{J_{w2} - J_p}{J_{w1}}\right) \times 100\% \quad (6)$$

$$DR_{ir} = \left(\frac{J_{w1} - J_{w2}}{J_{w1}}\right) \times 100\% \quad (7)$$

## 3. RESULTS AND DISCUSSION

**3.1. Near-Surface Elemental Composition.** The near-surface elemental composition of the fabricated membranes was investigated using XPS and the fitted C 1s regions were analyzed by CasaXPS processing software (Casa Software Ltd., U.K.). The results are shown in Figure 1. For PVDF1, fabricated using pure PVDF without additive, the surface composition consisted of carbon (54.47%), fluorine (44.96%), and oxygen (0.58%). The small oxygen signal may be caused by the absorption of $H_2O$ from the air.[12] The elemental compositions of PVDF2 and PVDF3 were similar, with oxygen ~13.0%, carbon ~61.5%, and fluorine ~25.5%. According to the FTIR, which were analyzed later, the unreacted PEGMA was totally washed out during the phase separation period. As shown in Table 4, the oxygen contents in PVDF2 and PVDF3 were significantly higher than that of PVDF1. The oxygen content derives from the additive PVDF-*g*-PEGMA. The higher the oxygen composition on the membrane surface, the


https://dx.doi.org/10.1021/acsomega.0c03429
ACS Omega 2020, 5, 23450–23459

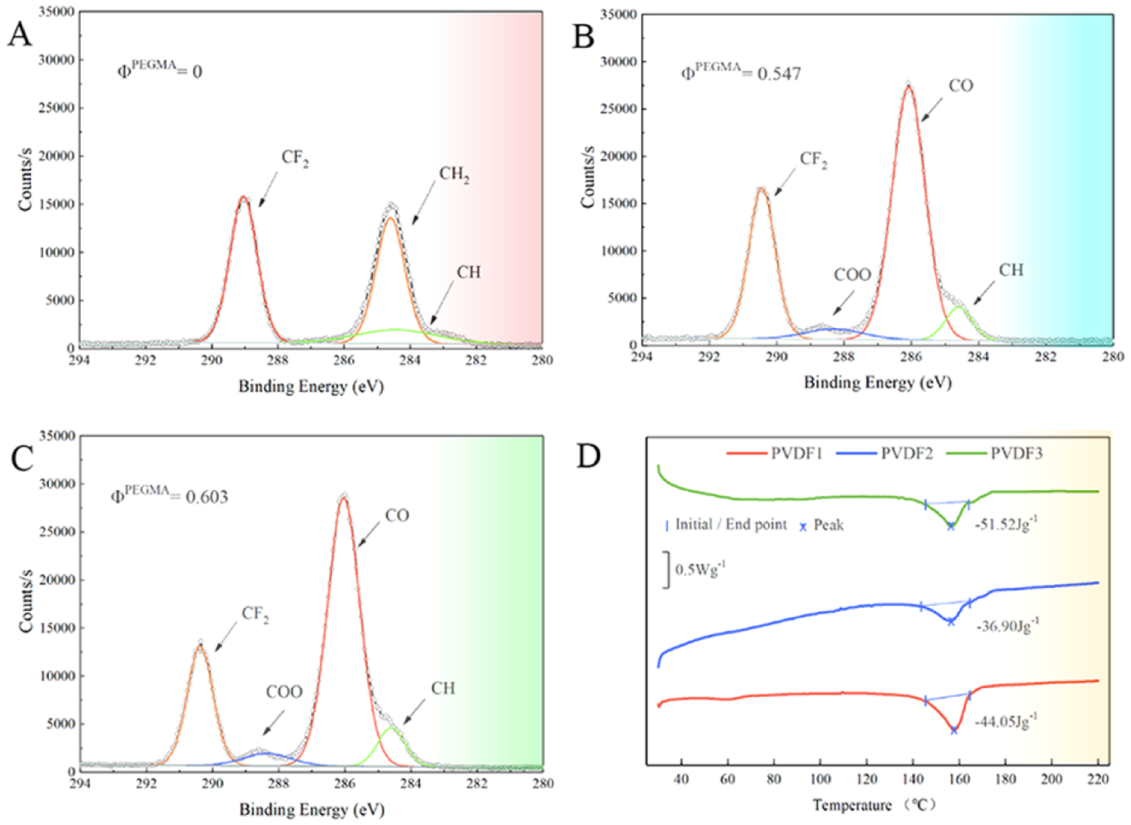


**Figure 1.** XPS spectra and fitted C 1s regions for: (A) PVDF1, (B) PVDF2, and (C) PVDF3 membranes. (D) DSC results. PVDF1: pure PVDF in NMP, PVDF2: PVDF-blended PVDF-*g*-PEGMA in DMAc, and PVDF3: PVDF-blended PVDF-*g*-PEGMA in NMP. The weight fractions of PEGMA are indicated in each graph.

**Table 4. Element Compositions on the Surface of the Fabricated Membranes Used in the Study**

| | element composition | | |
|---|---|---|---|
| membrane ID | C | O | F |
| PVDF1 | 54.47 | 0.58 | 44.96 |
| PVDF2 | 61.25 | 11.67 | 27.09 |
| PVDF3 | 61.66 | 14.26 | 24.07 |

more amphiphilic copolymer PVDF-*g*-PEGMA was migrated to the surface, leading to a more hydrophilic surface and affecting the performances of the fabricated membranes like antifouling. As for the fitted C 1s regions, the binding energies at 288.3 eV for O−C═O and 286.1 eV for C−O species in PEGMA were present in PVDF2 and PVDF3 membranes, indicating the successful blending of PVDF with PVDF-*g*-PEGMA, and hydrophilic PEGMA segments in PVDF-*g*-PEGMA migrated preferentially to the membrane surface.[30]

The fraction of PEGMA on the surface can be estimated using eq 8, where $A_{CF_2}$ and $A_{O-C=O}$ are the areas of the fitted $CF_2$ (289.1 eV) and O−C═O peaks, respectively. The weight fraction of PEGMA ($\phi_{PEGMA}$) was calculated using the molecular weights of PEGMA and PVDF.

$$X^{PEGMA} = \frac{A_{O-C=O}}{A_{CF_2} + A_{O-C=O}} \quad (8)$$

The results suggested that a larger quantity of PEGMA segments migrated more effectively to the surface of the membrane compared to previous studies.[18,19,30,31] During the phase separation periods, the hydrophilic PEGMA segments in PVDF-*g*-PEGMA migrated to the interface between water and polymer. As a result, the hydrophilic PEGMA segments tail-ends to end up on the membrane surface, which can be approved by the higher concentration of PVDF-*g*-PEGMA on the memrbrane surfaces than in casting solutions. This mechanism may be the result of a lower polymer concentration used in this study, which decreased the viscosity of the casting solution, thus reducing the exchange barrier between solvent and nonsolvent. More hydrophilic segments on the surface should increase the membrane wettability.

**3.2. Crystalline Phase of PVDF.** The crystalline phase of the membranes was analyzed using ATR-FTIR, the crystallinity was calculated using the results of DSC (Figure 1D), and the distribution of PVDF crystalline phases was surveyed with Raman analysis and subsequent estimation of the height ratio between peaks at 844 $cm^{-1}$ and at 801 $cm^{-1}$. The ATR-FTIR spectra are shown in Figure 2B. The bands at 1638 and 1727 $cm^{-1}$ represent the C═C and the C═O stretching band, respectively.[34,39] The existence of C═O and the absence of C═C in the spectra of PVDF2 and PVDF3 indicates the presence of reacted PEGMA segments, which in fact generated C═O bonds while breaking C═C bonds, and the removal of unreacted PEGMA containing the C═C band during polymer precipitation. This result also suggests that the PEGMA chains were successfully grafted onto PVDF.

ATR-FTIR spectra also provide an insight into the crystalline phases of PVDF. PVDF has four crystalline phases, $\alpha$, $\beta$, $\gamma$, and $\delta$, which influence its material properties.[40,41] The $\alpha$ crystalline phase can be represented by the characteristic absorption bands at 614, 764, 796, 855, and 976 $cm^{-1}$, while


https://dx.doi.org/10.1021/acsomega.0c03429
ACS Omega 2020, 5, 23450−23459

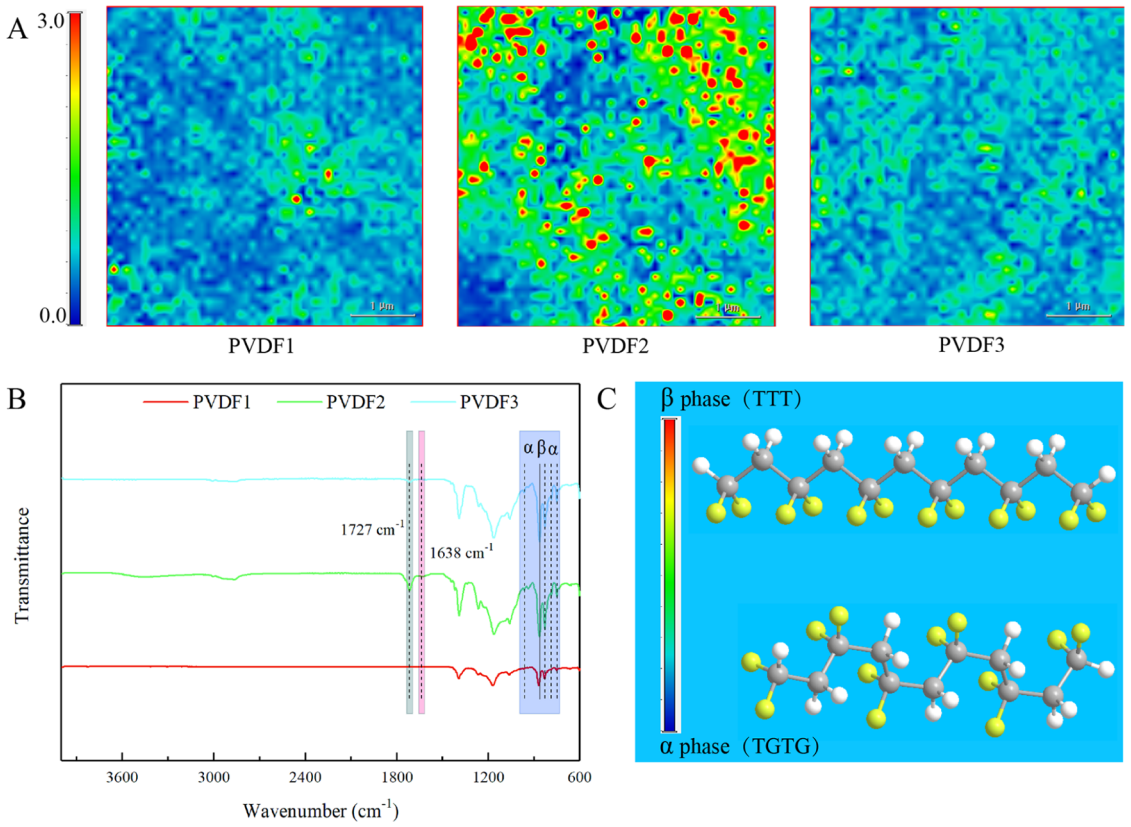


**Figure 2.** Results of PVDF crystallization. (A) The peak height ratio between 844/801 $cm^{-1}$ bands from Raman analysis. (B) ATR-FTIR spectra. (C) Schematic representation of $\alpha$ and $\beta$ crystal phases of PVDF. PVDF1: pure PVDF in NMP, PVDF2: PVDF-blended PVDF-*g*-PEGMA in DMAc, and PVDF3: PVDF-blended PVDF-*g*-PEGMA in NMP.

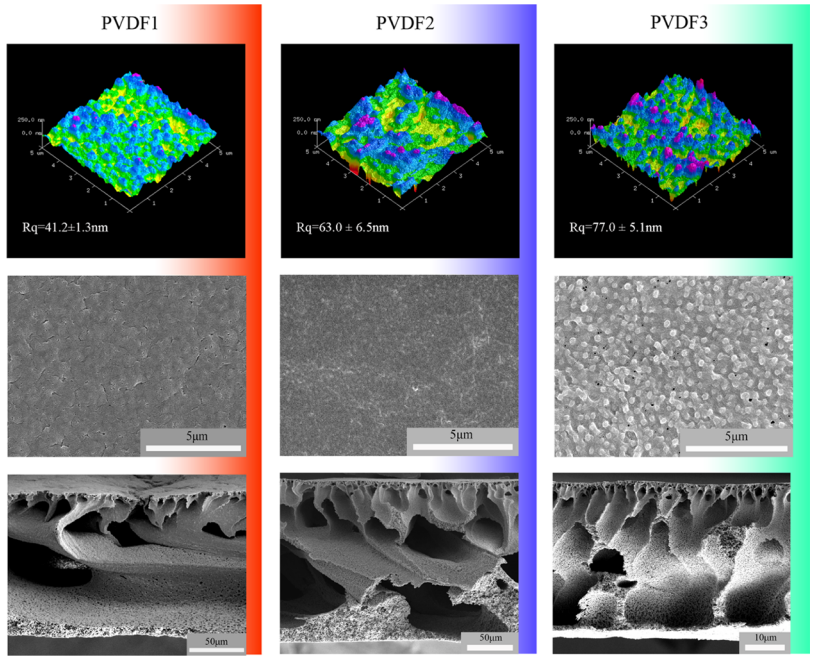


**Figure 3.** Characterization of the membrane surface and cross-section. PVDF1: pure PVDF in NMP, PVDF2: PVDF-blended PVDF-*g*-PEGMA in DMAc, and PVDF3: PVDF-blended PVDF-*g*-PEGMA in NMP. From top to bottom: AFM images, SEM micrographs of the surface, and SEM micrographs of the cross-sections.

the bands associated with the $\beta$ phase are located at 510 and 840 $cm^{-1}$; see Figure 2B.[42−44] Some characteristic absorption bands of the $\gamma$ phase at 512 and 840 $cm^{-1}$ are very similar to those of the $\beta$ phase; however, a $\gamma$ phase would be recognizable for the additional bands at 776, 812, and 833 $cm^{-1}$.[45] However, the characteristic bands of the $\gamma$ phase were absent from the



https://dx.doi.org/10.1021/acsomega.0c03429
*ACS Omega* 2020, 5, 23450−23459

Table 5. Properties of Fabricated Membranes: Surface Pore Size; Thickness; Total Porosity; Pure Water Permeability Coefficient; Permeability Indices Following Conditioning, Fouling with Sodium Alginate, and Recovery Based on Physical Cleaning

| membrane ID | $D_{ave}$ (nm) | $D_{max}$ (nm) | thickness ($\mu$m) | porosity (%) | pure water permeability (LMH/bar) | conditioning (LMH/bar) | SA solution (LMH/bar) | recovery (LMH/bar) |
|---|---|---|---|---|---|---|---|---|
| PVDF1[a] | 798.17 | 1743.23 | 246.8 | 78.34 | 1569.42 | 913.54 | 105.32 | 282.27 |
| PVDF2 | | | 134.6 | 95.21 | 675.26 | 585.40 | 139.89 | 523.64 |
| PVDF3 | 40.21 | 299.35 | 114.7 | 95.17 | 928.62 | 867.39 | 135.45 | 738.11 |

[a]Pores on PVDF1 are connected by cracks, $D_{ave}$ and $D_{max}$ are the lengths of the cracks.

spectra obtained in this study, and all of the membranes contained $\alpha$ and $\beta$ crystalline phases of PVDF. The temperature range of the solution can influence the formation of the PVDF crystalline phases.[46] The $\alpha$ phase can be obtained at any temperature of melting crystallization. However, when the solution crystallizes below 70 °C, the crystalline phase produced by the solidification of the polymer is the $\beta$ phase rather than the $\gamma$ phase. This mechanism explains the presence of the $\alpha$ and $\beta$ phases in the membranes.

As shown in Figure 1D, the melting enthalpy for PVDF1, PVDF2, and PVDF3 was 44.05, 36.90, and 51.52 J/g, respectively. The initial and end points of melting enthalpy of all of the fabricated membranes were practically the same, within the range of 145−164 °C; the peak point of pure PVDF was 157.8 °C, while that of the PVDF/PVDF-*g*-PEGMA membranes was 156.4 °C. The melting temperature of blended membranes decreased when compared with PVDF1.[47] The crystallinity of the fabricated membranes $X_c$ can be calculated by dividing the measured melting enthalpy change ($\Delta H_f$) by that of a perfect PVDF crystal $\Delta H_f^0$,[48] as shown in eq 9. The melting enthalpy of the perfect PVDF crystal is 105 J/g, as reported by Nakagawa and Ishida.[49] Therefore, the crystallinities of fabricated membranes were 41.95, 35.14, and 49.07%, respectively.

$$X_c = \frac{\Delta H_f}{\Delta H_f^0} \times 100\% \quad (9)$$

Further information on crystallinity was collected with Raman measurements. In Figure 2A, the band at 844 $cm^{-1}$ represents the $\beta$ crystalline phase of PVDF, while that at 801 $cm^{-1}$ represents the $\alpha$ crystalline phase. The peak height ratio, 844/801 $cm^{-1}$, intuitively provides an assessment of the distribution of PVDF crystalline phases of the fabricated membranes. The $\alpha$ phase was the dominating phase in the three fabricated membranes. The percentage of the $\beta$ phase was the highest in PVDF2, followed by PVDF3 and then PVDF1. The schematic representation of $\alpha$ and $\beta$ crystal phases of PVDF is reported in Figure 2C. The $\beta$ phase (TTT) molecules, with all-trans conformation, have the strongest polarity, that is, its dipoles all point in the same direction. The dipoles in the $\alpha$ phase (TGTG) are arranged in a way that they compensate, so the $\alpha$ phase is overall nonpolar.[50] The hydrophobicity of PVDF is mainly caused by the polarity of C−F. We hypothesize that, in the phase separation process, the C−F bonds pointed inward due to their hydrophobicity, thus decreasing the hydrophobicity of the membrane surface. As a result, the larger fraction of the $\beta$ phase in PVDF2 and PVDF3 membranes contributed to higher surface hydrophilicity for these membranes.

**3.3. Membrane Morphology.** The surface and cross-sectional morphologies of the membranes, as well as their roughness, are shown in Figure 3. Table 5 listed the average pore diameter ($D_{ave}$), maximum pore diameter ($D_{max}$), thickness, and porosity of the membranes. The absolute RMS surface roughness varied from 40 to 80 nm. These values are larger than those of PVDF-based membranes in previous studies.[18] This result is rationalized as more PVDF-*g*-PEGMA migrated to the membrane surface. This change caused membranes with larger RMS roughness.[18,31] The PVDF1 membrane showed cracks at the surface. These cracks were of different lengths and sizes on the surface of PVDF1, whereby some cracks connected and became defects on the membrane surface. The surface of PVDF2 and PVDF3 were more uniform, showing that the blending with PVDF-*g*-PEGMA improved the surface morphology; surface feature uniformity of ultrafiltration membranes is often argued as a necessary characteristic for enhanced performance, as it provides a sharper molecular weight cutoff curve. The few visible pores on the PVDF1 surface were connected by cracks, while the pores of PVDF2 membranes were too small for observation under the magnification of ×100k and smaller than what may influence the ultrafiltration performance. Furthermore, the surface of PVDF3 membranes showed that regular spherulite structures were because of the coexistence of NMP and PVDF-*g*-PEGMA in the casting solution, which was in accordance with previous studies.[18,19] The cross-sectional morphologies revealed instead that all of the membranes had a dense top layer and underlying macrovoids. The macrovoids of PVDF1 were significantly larger than those of PVDF2 and PVDF3; nevertheless, the overall porosity was higher for the blended membranes. The detailed porosity data are summarized in Table 5. The pore size and distribution, and the cross-section morphologies have a great influence on pure water flux, fouling, and the recovery test, which are described below.

**3.4. Wettability, Contact Angles, and Surface Free Energy.** The wettability of solid surfaces is generally measured by contact angle. The models to analyze such measurements mainly include Young's model, the Wenzel model, and the Cassie model.[51] According to the Wenzel model of wetting, chemically homogeneous rough surfaces increased the actual contact area of the "solid−liquid", making the surface to be greater than the apparent geometric contact area. As a result, the contact angle is reduced and the wetting of the membrane was enhanced. Due to the relatively large surface roughness of PVDF2 and PVDF3 surfaces, the Wenzel model is a better model to analyze contact angle data for these samples. When a water droplet falls on the membrane surface and fills the grooves, the relationship between the actual contact angle, $\theta'$, of the rough surface and the intrinsic contact angle, $\theta_c$, of the analogous smooth surface is described by eq 10.

$$\cos\theta' = r\cos\theta_c \quad (10)$$

Here, $r$ represents the roughness factor of the membrane surface and is estimated as the ratio of the actual surface area to


https://dx.doi.org/10.1021/acsomega.0c03429
ACS Omega 2020, 5, 23450−23459

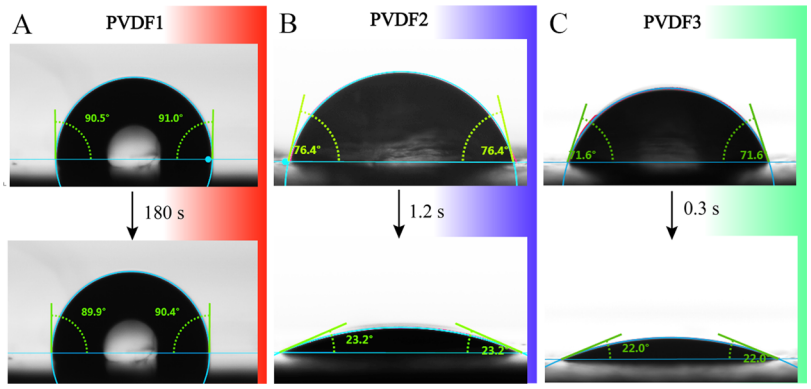


**Figure 4.** Images showing the change of the water contact angle in time on the surface of the membranes. (A) PVDF1: pure PVDF in NMP, (B) PVDF2: PVDF-blended PVDF-*g*-PEGMA in DMAc, and (C) PVDF3: PVDF-blended PVDF-*g*-PEGMA in NMP.

**Table 6. Details of the Surface Tensions of the Membranes Based on the XDLVO Theory**

| | polar liquid | $\Delta G_{sw}^{AB}$ | $\Delta G_{sp}^{AB}$ | $(\gamma^+)^{0.5}$ | $(\gamma^-)^{0.5}$ | $\gamma^{AB}$ | $\gamma^{LW}$ | $\gamma$ | average |
|---|---|---|---|---|---|---|---|---|---|
| PVDF1 | glycerol | −29.88 | −20.17 | 0.76 | 2.20 | 3.33 | 20.590 | 23.918 | 22.57955 |
| | ethylene glycol | −19.43 | −19.43 | 1.70 | 0.22 | 0.76 | | 21.351 | |
| | formamide | −22.33 | −22.33 | 1.64 | 0.57 | 1.88 | | 22.470 | |
| PVDF2 | glycerol | −38.88 | −11.05 | **−0.37**[a] | 4.22 | 3.16 | 27.457 | **30.619** | 27.60817 |
| | ethylene glycol | −5.50 | −5.50 | 0.48 | 0.06 | 0.06 | | 27.518 | |
| | formamide | −8.01 | −8.01 | 0.59 | 0.21 | 0.24 | | 27.699 | |
| PVDF3 | glycerol | −42.95 | 20.62 | **−3.35** | 7.60 | 50.87 | 33.313 | **84.182** | 34.27415 |
| | ethylene glycol | −6.01 | −6.01 | 0.53 | 0.07 | 0.07 | | 33.385 | |
| | formamide | −22.15 | −22.15 | 1.62 | 0.57 | 1.85 | | 35.163 | |

[a]Negative value of $(\gamma^+)^{0.5}$ and $(\gamma^-)^{0.5}$ is meaningless, indicating that the probe liquid was not suitable for the specific surface of interest.

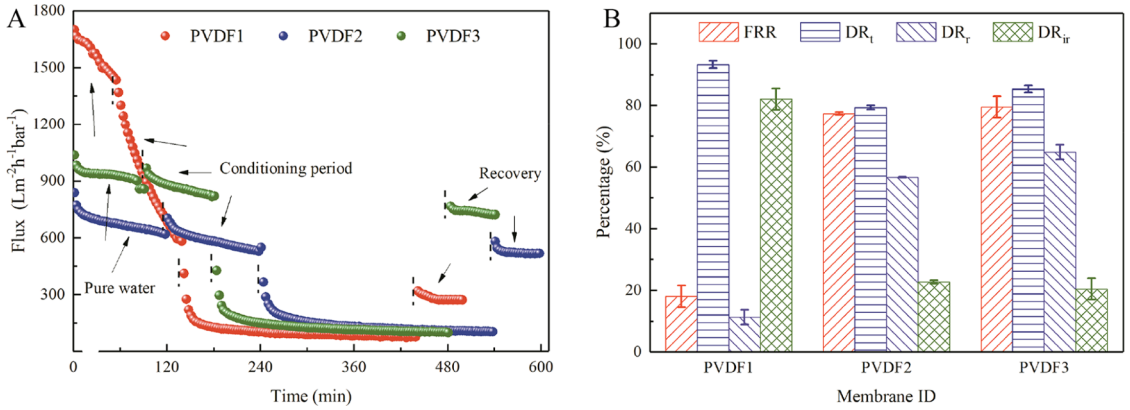


**Figure 5.** Membrane fouling behavior under filtration. (A) Measured permeate flux during the course of an experiment with varying feed solutions. (B) Fouling indices related to sodium alginate fouling. PVDF1: pure PVDF in NMP, PVDF2: PVDF-blended PVDF-*g*-PEGMA in DMAc, and PVDF3: PVDF-blended PVDF-*g*-PEGMA in NMP.

the apparent contact area; therefore, $r$ is ≥1. In this study, the blended membranes have a hydrophilic surface and $0° < \theta_c < 90°$. The high surface roughness may enhance its hydrophilicity, allowing the actual contact angle to decline rapidly, which is consistent with that observed in our study.[52] By changing the hydrophilicity and roughness of the membrane, the contact angle can be regulated with the goal to improve the membrane wettability.

The dynamic contact angle on the surface of the membranes is summarized in Figure 4. The average change on PVDF1 samples was small, from 90.7 to 90.1° in 3 min. In contrast, PVDF2 and PVDF3 showed superwettability behavior, with changes occurring rapidly. Specifically, the contact angles changed from 76.4 to 23.2° in 1.2 s and the water completely diffused into the membrane in 1.5 s for PVDF2 samples. Concerning PVDF3, the changes were even more rapid, from 71.6 to 22° in only 0.3 s, with total water infiltration in 0.5 s. These values are the average of 10 separate experiments. One of the reasons for this difference in wetting behavior is due to the blending of hydrophobic PVDF with PVDF-*g*-PEGMA, as more PEGMA segments were migrated to the surface of PVDF3 than that of PVDF2.[53] Whereas, more PEGMA segments contributed to a rougher surface of PVDF3.

More insight on this phenomenon was obtained by applying the surface free energy theory, whose results are summarized in Table 6. Please note that $(\gamma^+)^{0.5}$ of PVDF2 and PVDF3 calculated from measurements using glycerol as a second polar probe liquid was meaningless, suggesting that glycerol is not a


https://dx.doi.org/10.1021/acsomega.0c03429
ACS Omega 2020, 5, 23450−23459

suitable probe for these samples. The surface tensions determined for the membranes were 22.58 mJ/m$^2$ (PVDF1), 27.61 mJ/m$^2$ (PVDF2), and 34.27 mJ/m$^2$ (PVDF3). The results were consistent with experimental contact angle observations, suggesting that the wettability decreased in the order PVDF3 > PVDF2 > PVDF1. The values of free surface energy provide one more partial explanation of the wetting behavior of the membranes and the superwettability of the blended samples.

In summary, the modification with PVDF-*g*-PEGMA copolymers that preferentially migrated toward the surface and the increased polar $\beta$ crystalline phase of PVDF with preferred orientation increased the hydrophilicity of the membranes.[54] In addition, it has been proved that the solid surface heterogeneity and roughness significantly affect the air bubble/water droplet contact angle.[55−57] The high roughness of the blended membranes further enhanced their hydrophilicity, on the whole resulting in the high surface free energy of the fabricated membranes, resulting in rapid water spread on their surface and in the total water infiltration within the membrane in less than 1.2 s.

**3.5. Membrane Permeate Flux and Removal Efficiency.** The flux and the fouling behavior of the membranes were tested under the constant pressure of 0.07 MPa (0.7 bar). The values of membrane permeability are listed in Table 5, while the filtration results are shown in Figure 5. All of the membranes possessed a high water permeability, with PVDF1 showing the highest water flux at the beginning of the fouling tests, which, however, dropped sharply within the first 2 h of the compaction period. The high flux of PVDF1 is mainly attributed to the numerous defective cracks observed on the surface and to the large cross-sectional pores that allow easy water transport across the membrane, which are shown in Table 5 and Figure 3. The flux of PVDF2 and PVDF3 was more stable compared to the pure PVDF1 membrane during the initial filtration with pure water. After varying degrees of flux decline during the subsequent conditioning and fouling periods, all of the membranes reached a near-steady-state flux value of approximately 100 L m$^{-2}$ h$^{-1}$. Please note that the SA rejection rates of the membranes were 55.3 ± 4.3% (PVDF1), 69.2 ± 3.2% (PVDF2), and 82.9 ± 3.2% (PVDF3).

Important differences in flux recovery were observed following physical cleaning, the order of observed flux was PVDF3 > PVDF2 ≫ PVDF1 at the end of the fouling experiments. The fouling indices shown in Figure 5B allow a more direct comparison of the fouling behavior of the membranes. High $DR_r/DR_t$ means relatively reversible fouling, thus better antifouling properties can be represented by higher values of FRR and $DR_r/DR_t$.[58] FRR and $DR_r/DR_t$ ratios decreased in the order PVDF3 (79.53 and 76.02%) > PVDF2 (77.34 and 71.44%) ≫ PVDF1 (17.99 and 12.08%). Therefore, the blended membranes exhibited remarkably better flux recovery performance compared to PVDF1. Overall, PVDF3 performed better than all of the other membranes, due most likely to the best combination of the surface morphology and porosity, overall porosity, and surface wetting behavior. Also, higher wettability translated directly into higher the SA rejection rates and flux recovery rates, indicating that the hydrophilic segments at the membrane surface contributed greatly to the enhancement of performance. The two fabricated membranes with superwettability behavior had high water permeability, a high FRR of nearly 80%, and remarkable antifouling performance, suggesting their potential in the practical applications.

## 4. CONCLUSIONS

In summary, superwettability behavior was observed for PVDF-based membranes blended with PVDF-*g*-PEGMA copolymers. This behavior was the result of the synergetic effect of the following factors: (i) the successful blending of PVDF with amphiphilic copolymer PVDF-*g*-PEGMA; higher content of PVDF-*g*-PEGMA on the surface improves the hydrophilicity of the fabricated membranes. (ii) The proportion of PVDF in the $\beta$ crystalline phase increased on the membrane surface, which reduced the hydrophobicity of the surface. (iii) The higher surface roughness of the blended membranes enlarged the actual contact area between water and membrane significantly, which further increased the membrane wettability according to the Wenzel model of wetting. (iv) The blended membranes were characterized by high surface energy, which promotes the interaction of water with the surface. The factors (i) and (ii) combined and significantly increased the wettability of the membranes. Macroscopically, these parameters result in the rapid wetting and uptake of water by the membrane, with water droplets being completely flattened or infiltrated within 0.5 s for the best fabricated membranes. The two membranes with superwettability behavior showed high performance in flux and antifouling experiments under ultrafiltration conditions. Hydrophobicity is the current bottleneck of PVDF membranes that limits their further applications in water treatment processes. This study discusses how a simple approach can be pursued to produce membranes that are based on the same chemically and mechanically stable PVDF chemistry, but with the added property of being superwettable.

## AUTHOR INFORMATION


### Corresponding Author

**Baicang Liu** − *Key Laboratory of Deep Earth Science and Engineering (Ministry of Education), College of Architecture and Environment, Institute of New Energy and Low-Carbon Technology, Sichuan University, Chengdu, Sichuan 610207, P. R. China*; orcid.org/0000-0003-3219-1924; Phone: +86-28-85995998; Email: bcliu@scu.edu.cn, baicangliu@gmail.com; Fax: +86-28-62138325

### Authors

**Qidong Wu** − *Key Laboratory of Deep Earth Science and Engineering (Ministry of Education), College of Architecture and Environment, Institute of New Energy and Low-Carbon Technology, Sichuan University, Chengdu, Sichuan 610207, P. R. China*

**Alberto Tiraferri** − *Department of Environment, Land and Infrastructure Engineering, Politecnico di Torino, 10129 Turin, Italy*; orcid.org/0000-0001-9859-1328

**Tong Li** − *Key Laboratory for Water Quality and Conservation of the Pearl River Delta, Ministry of Education, Institute of Environmental Research at Greater Bay, Guangzhou University, Guangzhou 510006, P. R. China*

**Wancen Xie** − *Key Laboratory of Deep Earth Science and Engineering (Ministry of Education), College of Architecture and Environment, Institute of New Energy and Low-Carbon Technology, Sichuan University, Chengdu, Sichuan 610207, P. R. China*




https://dx.doi.org/10.1021/acsomega.0c03429
ACS Omega 2020, 5, 23450−23459

**Haiqing Chang** − *Key Laboratory of Deep Earth Science and Engineering (Ministry of Education), College of Architecture and Environment, Institute of New Energy and Low-Carbon Technology, Sichuan University, Chengdu, Sichuan 610207, P. R. China*

**Yuhua Bai** − *Infrastructure Construction Department, Chengdu University, Chengdu, Sichuan 610106, P. R. China*

Complete contact information is available at: https://pubs.acs.org/10.1021/acsomega.0c03429

### Notes

The authors declare no competing financial interest.

## ■ ACKNOWLEDGMENTS

This work was supported by the National Natural Science Foundation of China (51678377, 51708371), the State Key Laboratory of Separation Membranes and Membrane Processes (Tianjin Polytechnic University) (M2-201809), the Fundamental Research Funds for the Central Universities and Sichuan University and Yibin City People's Government strategic cooperation project (2019CDYB-25). A.T. acknowledges the support of Politecnico di Torino. The authors thank Shaolan Wang at Analytical & Testing Center, Sichuan University for DSC measurements. The views and ideas expressed herein are solely those of the authors and do not represent the ideas of the funding agencies in any form.

## ■ REFERENCES

(1) Kang, G.-d.; Cao, Y.-m. Application and modification of poly(vinylidene fluoride) (PVDF) membranes - A review. *J. Membr. Sci.* **2014**, *463*, 145−165.

(2) Hashim, N. A.; Liu, Y.; Li, K. Preparation of PVDF Hollow Fiber Membranes Using SiO2 Particles: The Effect of Acid and Alkali Treatment on the Membrane Performances. *Ind. Eng. Chem. Res.* **2011**, *50*, 3035−3040.

(3) Qing, Y.; Yang, C.; Yu, N.; Shang, Y.; Sun, Y.; Wang, L.; Liu, C. Superhydrophobic TiO2/polyvinylidene fluoride composite surface with reversible wettability switching and corrosion resistance. *Chem. Eng. J.* **2016**, *290*, 37−44.

(4) Zeng, G.; He, Y.; Zhan, Y.; Zhang, L.; Pan, Y.; Zhang, C.; Yu, Z. Novel polyvinylidene fluoride nanofiltration membrane blended with functionalized halloysite nanotubes for dye and heavy metal ions removal. *J. Hazard. Mater.* **2016**, *317*, 60−72.

(5) Gopi, S.; Kargl, R.; Kleinschek, K. S.; Pius, A.; Thomas, S. Chitin nanowhisker - Inspired electrospun PVDF membrane for enhanced oil-water separation. *J. Environ. Manage.* **2018**, *228*, 249−259.

(6) Zhang, L. Q.; Zhu, Z. K.; Azhar, U.; Ma, J. C.; Zhang, Y. B.; Zong, C. Y.; Zhang, S. X. Synthesis of Well-Defined PVDF-Based Amphiphilic Block Copolymer via Iodine Transfer Polymerization for Antifouling Membrane Application. *Ind. Eng. Chem. Res.* **2018**, *57*, 8689−8697.

(7) Pourziad, S.; Omidkhah, M. R.; Abdollahi, M. Improved antifouling and self-cleaning ability of PVDF ultrafiltration membrane grafted with polymer brushes for oily water treatment. *J. Ind. Eng. Chem.* **2020**, *83*, 401−408.

(8) Gopakumar, D. A.; Pasquini, D.; Henrique, M. A.; de Morais, L. C.; Grohens, Y.; Thomas, S. Meldrum's Acid Modified Cellulose Nanofiber-Based Polyvinylidene Fluoride Microfiltration Membrane for Dye Water Treatment and Nanoparticle Removal. *ACS Sustainable Chem. Eng.* **2017**, *5*, 2026−2033.

(9) Shi, Q.; Su, Y. L.; Ning, X.; Chen, W. J.; Peng, J. M.; Jiang, Z. Y. Graft polymerization of methacrylic acid onto polyethersulfone for potential pH-responsive membrane materials. *J. Membr. Sci.* **2010**, *347*, 62−68.

(10) Mansourpanah, Y.; Kakanejadifard, A.; Dehrizi, F. G.; Tabatabaei, M.; Afarani, H. S. Increasing and enhancing the performance and antifouling characteristics of PES membranes using acrylic acid and microwave-modified chitosan. *Korean J. Chem. Eng.* **2015**, *32*, 149−158.

(11) Ndlwana, L.; Sikhwivhilu, K.; Moutloali, R.; Ngila, J. C. Microwave-assisted graft synthesis and characterization of poly-(methacrylic acid)-grafted polyethersulfone towards dense hydrophilic and low-fouling membranes for water treatment. *Phys. Chem. Earth* **2018**, *106*, 107−115.

(12) Wu, H.; Li, T.; Liu, B.; Chen, C.; Wang, S.; Crittenden, J. C. Blended PVC/PVC-g-PEGMA ultrafiltration membranes with enhanced performance and antifouling properties. *Appl. Surf. Sci.* **2018**, *455*, 987−996.

(13) Ashjari, H. R.; Ahmadi, A.; Dorraji, M. S. S. Synthesis and employment of PEGDA for fabrication of superhydrophilic PVDF/PEGDA electrospun nanofibrous membranes by in-situ visible photopolymerization. *Korean J. Chem. Eng.* **2018**, *35*, 289−297.

(14) Li, M.; Li, J.; Zhou, M.; Xian, Y.; Shui, Y.; Wu, M.; Yao, Y. Super-hydrophilic electrospun PVDF/PVA-blended nanofiber membrane for microfiltration with ultrahigh water flux. *J. Appl. Polym. Sci.* **2020**, *137*, No. 48416.

(15) Yang, B.; Yang, X.; Liu, B.; Chen, Z.; Chen, C.; Liang, S.; Chu, L.-Y.; Crittenden, J. PVDF blended PVDF-g-PMAA pH-responsive membrane: Effect of additives and solvents on membrane properties and performance. *J. Membr. Sci.* **2017**, *541*, 558−566.

(16) Ran, J.; Wu, L.; Zhang, Z.; Xu, T. Atom transfer radical polymerization (ATRP): A versatile and forceful tool for functional membranes. *Prog. Polym. Sci.* **2014**, *39*, 124−144.

(17) Matyjaszewski, K. Advanced Materials by Atom Transfer Radical Polymerization. *Adv. Mater.* **2018**, *30*, No. 1706441.

(18) Liu, B.; Chen, C.; Li, T.; Crittenden, J.; Chen, Y. High performance ultrafiltration membrane composed of PVDF blended with its derivative copolymer PVDF-g-PEGMA. *J. Membr. Sci.* **2013**, *445*, 66−75.

(19) Chen, C.; Tang, L.; Liu, B.; Zhang, X.; Crittenden, J.; Chen, K. L.; Chen, Y. Forming mechanism study of unique pillar-like and defect-free PVDF ultrafiltration membranes with high flux. *J. Membr. Sci.* **2015**, *487*, 1−11.

(20) Van Oss, C. J. Use of the combined Lifshitz-van der Waals and Lewis acid-base approaches in determining the apolar and polar contributions to surface and interfacial tensions and free energies. *J. Adhes. Sci. Technol.* **2002**, *16*, 669−677.

(21) Subhi, N.; Verliefde, A. R. D.; Chen, V.; Le-Clech, P. Assessment of physicochemical interactions in hollow fibre ultrafiltration membrane by contact angle analysis. *J. Membr. Sci.* **2012**, *403−404*, 32−40.

(22) Bormashenko, E. Progress in understanding wetting transitions on rough surfaces. *Adv. Colloid Interface Sci.* **2015**, *222*, 92−103.

(23) Papadopoulos, P.; Mammen, L.; Deng, X.; Vollmer, D.; Butt, H.-J. How superhydrophobicity breaks down. *Proc. Natl. Acad. Sci. U.S.A.* **2013**, *110*, 3254−3258.

(24) Celia, E.; Darmanin, T.; de Givenchy, E. T.; Amigoni, S.; Guittard, F. Recent advances in designing superhydrophobic surfaces. *J. Colloid Interface Sci.* **2013**, *402*, 1−18.

(25) Wang, R.; Zhao, X.; Jia, N.; Cheng, L.; Liu, L.; Gao, C. Superwetting Oil/Water Separation Membrane Constructed from In Situ Assembled Metal-Phenolic Networks and Metal-Organic Frameworks. *ACS Appl. Mater. Interfaces* **2020**, *12*, 10000−10008.

(26) Wu, Q.; Tiraferri, A.; Wu, H.; Xie, W.; Liu, B. Improving the Performance of PVDF/PVDF-g-PEGMA Ultrafiltration Membranes by Partial Solvent Substitution with Green Solvent Dimethyl Sulfoxide during Fabrication. *ACS Omega* **2019**, *4*, 19799−19807.

(27) Zhao, X. J.; Cheng, J.; Chen, S. J.; Zhang, J.; Wang, X. L. Hydrophilic modification of poly(vinylidene fluoride) (PVDF) by in situ polymerization of methyl methacrylate (MMA) monomer. *Colloid Polym. Sci.* **2010**, *288*, 1327−1332.

(28) Bi, Q. Y.; Li, Q.; Tian, Y.; Lin, Y. K.; Wang, X. L. Hydrophilic modification of poly(vinylidene fluoride) membrane with poly(vinyl pyrrolidone) via a cross-linking reaction. *J. Appl. Polym. Sci.* **2013**, *127*, 394−401.

(29) Lim, S. J.; Shin, I. H. Graft copolymerization of GMA and EDMA on PVDF to hydrophilic surface modification by electron beam irradiation. *Nucl. Eng. Technol.* **2020**, *52*, 373−380.
(30) Wang, S.; Li, T.; Chen, C.; Liu, B.; Crittenden, J. C. PVDF ultrafiltration membranes of controlled performance via blending PVDF-g-PEGMA copolymer synthesized under different reaction times. *Front. Environ. Sci. Eng.* **2018**, *12*, No. 3.
(31) Wang, S.; Li, T.; Chen, C.; Chen, S.; Liu, B.; Crittenden, J. Non-woven PET fabric reinforced and enhanced the performance of ultrafiltration membranes composed of PVDF blended with PVDF-g-PEGMA for industrial applications. *Appl. Surf. Sci.* **2018**, *435*, 1072−1079.
(32) Chen, G. E.; Sun, W. G.; Kong, Y. F.; Wu, Q.; Sun, L.; Yu, J.; Xu, Z. L. Hydrophilic Modification of PVDF Microfiltration Membrane with Poly (Ethylene Glycol) Dimethacrylate through Surface Polymerization. *Polym.-Plast. Technol. Eng.* **2018**, *57*, 108−117.
(33) Zhao, P.; Bai, Y.; Liu, B.; Chang, H.; Cao, Y.; Fang, J. Process optimization for producing ultrapure water with high resistivity and low total organic carbon. *Process Saf. Environ. Prot.* **2019**, *126*, 232−241.
(34) Hashim, N. A.; Liu, F.; Li, K. A simplified method for preparation of hydrophilic PVDF membranes from an amphiphilic graft copolymer. *J. Membr. Sci.* **2009**, *345*, 134−141.
(35) Kim, H.-C.; Dempsey, B. A. Membrane fouling due to alginate, SMP, EfOM, humic acid, and NOM. *J. Membr. Sci.* **2013**, *428*, 190−197.
(36) Huang, F. L.; Wang, Q. Q.; Wei, Q. F.; Gao, W. D.; Shou, H. Y.; Jiang, S. D. Dynamic wettability and contact angles of poly(vinylidene fluoride) nanofiber membranes grafted with acrylic acid. *eXPRESS Polym. Lett.* **2010**, *4*, 551−558.
(37) Hwang, G.; Yang, J.-h.; Lee, C.-H.; Ahn, I.-S.; Mhin, B. J. New Selection Criterion for a Base Polar Liquid in the Lifshitz-van der Waals/Lewis Acid-Base Approach. *J. Phys. Chem. C* **2011**, *115*, 12458−12463.
(38) Zhao, Q.; Xie, R.; Luo, F.; Faraj, Y.; Liu, Z.; Ju, X.-J.; Wang, W.; Chu, L.-Y. Preparation of High Strength Poly(vinylidene fluoride) Porous Membranes with Cellular Structure via Vapor-Induced Phase Separation. *J. Membr. Sci.* **2018**, *549*, 151−164.
(39) Xie, W.; Li, T.; Chen, C.; Wu, H.; Liang, S.; Chang, H.; Liu, B.; Drioli, E.; Wang, Q.; Crittenden, J. C. Using the Green Solvent Dimethyl Sulfoxide To Replace Traditional Solvents Partly and Fabricating PVC/PVC-g-PEGMA Blended Ultrafiltration Membranes with High Permeability and Rejection. *Ind. Eng. Chem. Res.* **2019**, *58*, 6413−6423.
(40) Sencadas, V.; Gregorio, R.; Lanceros-Mendez, S. Processing and characterization of a novel nonporous poly(vinilidene fluoride) films in the beta phase. *J. Non-Cryst. Solids* **2006**, *352*, 2226−2229.
(41) Lederle, F.; Harter, C.; Beuermann, S. Inducing beta phase crystallinity of PVDF homopolymer, blends and block copolymers by anti-solvent crystallization. *J. Fluorine Chem.* **2020**, *234*, No. 109522.
(42) Gregorio, R. Determination of the alpha, beta, and gamma crystalline phases of poly(vinylidene fluoride) films prepared at different conditions. *J. Appl. Polym. Sci.* **2006**, *100*, 3272−3279.
(43) Chang, H.; Li, T.; Liu, B.; Chen, C.; He, Q.; Crittenden, J. C. Smart ultrafiltration membrane fouling control as desalination pretreatment of shale gas fracturing wastewater: The effects of backwash water. *Environ. Int.* **2019**, *130*, 104869.
(44) Zheng, Y. R.; Zhang, J.; Sun, X. L.; Li, H. H.; Ren, Z. J.; Yan, S. K. Crystal Structure Regulation of Ferroelectric Poly(vinylidene fluoride) via Controlled Melt-Recrystallization. *Ind. Eng. Chem. Res.* **2017**, *56*, 4580−4587.
(45) Benz, M.; Euler, W. B. Determination of the crystalline phases of poly(vinylidene fluoride) under different preparation conditions using differential scanning calorimetry and infrared spectroscopy. *J. Appl. Polym. Sci.* **2003**, *89*, 1093−1100.
(46) Kang, S. J.; Park, Y. J.; Sung, J.; Jo, P. S.; Park, C.; Kim, K. J.; Cho, B. O. Spin cast ferroelectric beta poly(vinylidene fluoride) thin films via rapid thermal annealing. *Appl. Phys. Lett.* **2008**, *92*, No. 012921.
(47) Liu, F.; Hashim, N. A.; Liu, Y.; Abed, M. R. M.; Li, K. Progress in the production and modification of PVDF membranes. *J. Membr. Sci.* **2011**, *375*, 1−27.
(48) Guo, Q. P. Completely Miscible Ternary Blends .3. Poly(vinylidene fluoride)-Poly(methyl methacrylate)-Poly(vinyl acetate). *Eur. Polym. J.* **1996**, *32*, 1409−1413.
(49) Nakagawa, K.; Ishida, Y. Annealing Effects in Poly(vinylidene fluoride) as Revealed by Specific Volume Measurements, Differential Scanning Calorimetry, and Electron Microscopy. *J. Polym. Sci., Polym. Phys. Ed.* **1973**, *11*, 2153−2171.
(50) Voet, V. S. D.; ten Brinke, G.; Loos, K. Well-Defined Copolymers Based on Poly(vinylidene fluoride): From Preparation and Phase Separation to Application. *J. Polym. Sci., Part A: Polym. Chem.* **2014**, *52*, 2861−2877.
(51) Whyman, G.; Bormashenko, E.; Stein, T. The rigorous derivation of Young, Cassie-Baxter and Wenzel equations and the analysis of the contact angle hysteresis phenomenon. *Chem. Phys. Lett.* **2008**, *450*, 355−359.
(52) Liu, M. J.; Zheng, Y. M.; Zhai, J.; Jiang, L. Bioinspired Super-antiwetting Interfaces with Special Liquid-Solid Adhesion. *Acc. Chem. Res.* **2010**, *43*, 368−377.
(53) Shen, J.; Zhang, Q.; Yin, Q.; Cui, Z.; Li, W.; Xing, W. Fabrication and Characterization of Amphiphilic PVDF Copolymer Ultrafiltration Membrane With High Anti-Fouling Property. *J. Membr. Sci.* **2017**, *521*, 95−103.
(54) Younas, H.; Bai, H.; Shao, J.; Han, Q.; Ling, Y.; He, Y. Super-Hydrophilic and Fouling Resistant PVDF Ultrafiltration Membranes Based on A Facile Prefabricated Surface. *J. Membr. Sci.* **2017**, *541*, 529−540.
(55) Vogler, E. A. Structure and reactivity of water at biomaterial surfaces. *Adv. Colloid Interface Sci.* **1998**, *74*, 69−117.
(56) Tang, K.; Wang, X.; Yan, W.; Yu, J.; Xu, R. Fabrication of superhydrophilic Cu2O and CuO membranes. *J. Membr. Sci.* **2006**, *286*, 279−284.
(57) Yuan, J.; Liu, X.; Akbulut, O.; Hu, J.; Suib, S. L.; Kong, J.; Stellacci, F. Superwetting nanowire membranes for selective absorption. *Nat. Nanotechnol.* **2008**, *3*, 332−336.
(58) Xu, Z.; Liao, J.; Tang, H.; Efome, J. E.; Li, N. Preparation and Antifouling Property Improvement of Troger's base Polymer Ultrafiltration Membrane. *J. Membr. Sci.* **2018**, *561*, 59−68.


https://dx.doi.org/10.1021/acsomega.0c03429
*ACS Omega* 2020, 5, 23450−23459